J Neurooncol (2014) 119:297–306
DOI 10.1007/s11060-014-1514-2

LABORATORY INVESTIGATION

In vivo and ex vivo assessment of the blood brain barrier integrity in different glioblastoma animal models

Cindy Leten · Tom Struys · Tom Dresselaers · Uwe Himmelreich

Received: 17 February 2014 / Accepted: 18 June 2014 / Published online: 3 July 2014

Abstract Blood brain barrier (BBB) disruption is used (pre)clinically as a measure for brain tumor malignancy and grading. During treatment it is one of the parameters followed rigorously to assess therapeutic efficacy. In animal models, both invasive and non-invasive methods are used to determine BBB disruption, among them Evans blue injection prior to sacrifice and T1-weighted magnetic resonance imaging (MRI) post contrast injection. In this study, we have assessed the BBB integrity with the methods mentioned above in two experimental high grade glioma models, namely the GL261 mouse glioblastoma model and the Hs683 human oligodendroglioma model. The GL261 model showed clear BBB integrity loss with both, contrast-enhanced (CE) MRI and Evans blue staining. In contrast, the Hs683 model only displayed BBB disruption with CE-MRI, which was not evident on Evans blue staining, indicating a limited BBB disruption. These results clearly indicate the importance of assessing the BBB integrity status using appropriate methods. Especially when using large therapeutic molecules that have difficulties crossing the BBB, care should be taken with the appropriate BBB disruption assessment studies.

C. Leten · T. Struys · T. Dresselaers · U. Himmelreich (✉)
Department of Imaging and Pathology, Biomedical MRI, KU Leuven, O&N1, Herestraat 49, P.O. Box 505, 3000, Louvain, Belgium
e-mail: Uwe.Himmelreich@med.kuleuven.be

C. Leten · T. Dresselaers · U. Himmelreich
Molecular Small Animal Imaging Center, KU Leuven, 3000 Louvain, Belgium

T. Struys
Biomedical Research Institute Lab of Histology, University Hasselt, 3500 Hasselt, Belgium

Keywords Magnetic resonance imaging · Blood brain barrier · Glioma · Animal model · Contrast agent

Introduction

One of the characteristics of high grade gliomas is angiogenesis as tumors rely on both co-option of existing blood vessels and neovascularization to meet their oxygen and nutrient requirements [1]. Only specific, carrier mediated transport is possible in the normal brain. Under pathological conditions, both transcellular and paracellular transport increase, thus allowing passage of substances into the brain that normally do not cross an intact blood brain barrier (BBB) [2, 3].

In humans, neovascularization is correlated with tumor grade and malignancy. Therefore, T1-weighted (T1 W) magnetic resonance imaging (MRI) after injection of contrast agents like gadolinium chelates, such as Dotarem® (MW 562 Da) is performed on a regular basis to assess the BBB integrity and diagnose high-grade gliomas [4]. Accumulation of these paramagnetic chelates in the brain indicates loss of BBB integrity as they normally do not cross the BBB. Contrast enhanced MRI (CE-MRI) has mostly replaced CT for non-invasive BBB integrity assessment as MRI shows higher soft tissue contrast compared to CT [5, 6].

In a preclinical setting, several low and high molecular weight vascular permeability markers are available to assess the BBB integrity [3]. Both radiolabeled markers including alpha-aminoisobutyric acid, sucrose and inulin [7, 8] and non-radioactive low molecular markers such as sodium fluorescein were developed for ex vivo assessment of the BBB integrity. Furthermore, high molecular weight markers were developed including horseradish peroxidase,

dextran and Evans blue [3]. The non-toxic Evans blue (MW 961) binds to albumin (Evans blue–Albumin: MW 69,000 Da) directly after intravenous injection and is therefore contained to the blood stream. When sites of BBB disruption are present, Evans blue crosses the BBB, thus resulting in site-specific accumulation [3]. Unfortunately, to assess the BBB disruption with such low or high molecular weight dyes, animals need to be sacrificed and brain sections analyzed, which is labor intensive and requires large numbers of animals as longitudinal studies on individual animals are impossible. In addition to histological methods, non-invasive CE-MRI protocols using injection of gadolinium chelates, similar to the protocols used in humans have been developed for dedicated small animal MRI [4, 9, 10] hereby, facilitating longitudinal studies on a small number of animals.

The loss of the BBB integrity is both in humans and experimental glioma models one of the characteristics used to assess and follow-up therapeutic response of glioblastoma. Furthermore, the effectiveness of some experimental treatments, such as systemic delivery of cells [11, 12] or administration of large or hydrophilic compounds [13] usually depends on the disruption of the BBB. It is therefore crucial to characterize the vascular integrity of tumor models very carefully before assessing novel treatment approaches.

In this study, we compared two brain tumor models in mice for the disruption of the BBB. The most frequently used glioblastoma mouse model is the GL261 model, which has been well described [14] with a documented BBB disruption [10]. The less studied humanized Hs683 oligodendroglioma model [15] was selected to validate to what extent it meets the hallmarks of glioblastoma models like the disruption of the BBB integrity.

Materials and methods

Mice and stereotactical injections

The GL261 cell line, a mouse glioblastoma model, was obtained from Dr S. Van Gool, University of Leuven, Belgium. The Hs683 cell line, derived from a human oligodendroglioma, was obtained from Dr R. Kiss, University of bruxelles, Belgium. All animal experiments were conducted according to the european union community council guidelines and were approved by the local ethics committee of Ku Leuven. Animals were anaesthetized by an i.p. injection of a ketamine (ceva, Pompidou, France, 4.5 mg/kg)/medetomidin (Domitor®, pfizer, New york, USA, 0.6 mg/kg) mixture. Local analgesia (2 % xylocain, astrazeneca, London, UK) and antibiotics (6 mg/mouse, ampiveto-20 (200 mg/ml), VMD, new haw, Surrey, UK) were administered prior to surgery. After fixation of the animals in a stereotactic frame adapted with a quintessential stereotaxic injector (both from stoelting, wood dale USA), cells were injected (speed: 0.5 µl/min) into the right striatum of C57Bl6/j mice at the following coordinates: 0.5 mm anterior and 2.0 mm lateral to bregma and 3.0 mm from the dura using a 10 µl Hamilton syringe, equipped with a 22 G needle. 2.5×10^5 GL261 cells or 5×10^4 Hs683 cells were injected in C57Bl6/j (N = 12) or Hsd: Athymic Nud—Foxn ^{1nu}mice (N = 22) (Harlan laboratories, indianapolis, Indiana, USA), respectively.

MRI

All MR images were acquired with a 9.4T Biospec small animal MR scanner (Bruker Biospin, Ettlingen, Germany) equipped with a horizontal bore magnet and an actively shielded gradient set of 600mT/m (117 mm inner diameter) using a 7 cm linearly polarized resonator for transmission and an actively decoupled dedicated mouse surface coil for receiving (rapid biomedical, Rimpar, Germany). MRI was performed once per week to follow-up tumor growth and BBB integrity. Prior to scanning, mice were anaesthetized with 2 % isoflurane for induction and 1.5 % isoflurane for maintenance, respectively. Temperature and respiration were monitored throughout the experiment and maintained at 37 °C and 100–120 breaths/min. T2-weighted (T2 W) MRI scans (rapid acquisition with refocused echoes (RARE) sequence, repetition time (TR):3000 ms, effective echo time (TE):50.2 ms, RARE factor: 9, matrix size: 256 × 256, field of view (FOV): 2 × 2 cm, number of continuous slices: 16, slice orientation: coronal, slice thickness: 0.5 cm, in plane resolution: 78 µm^2) were used to monitor tumor growth. The area of the tumor was determined by outlining it manually on all slices of the T2 W MR images with coronal orientation using the Paravision 5.1 software (Bruker, Biospin). The sum of the cross sectional discs was used to determine total tumor volumes. To validate the integrity of the blood brain barrier, pre- and post-contrast (gadolinium (Dotarem®), guerbet, Villepinte, France, dosage: 100 µl/mouse of 0.05 mmol/ml, i.v.) T1 W MR images were acquired (RARE sequence, RARE factor: 4, TR: 819 ms, TE: 7.6 ms, matrix size: 256 × 256, FOV: 2 × 2 cm, number of slices: 20, slice thickness: 0.5 mm, orientation: axial, in plane resolution: 78 µm^2). The relative signal intensity of the tumor region showing the strongest contrast enhancement (relative to surrounding brain tissue) was determined by placing a region of interest (ROI) over the area using the Paravision 5.1. software. To avoid influences from strong tumor heterogeneity (necrosis), we analyzed tumor regions with strong contrast enhancements after manual delineation. For statistical analysis of the BBB integrity, pre-

contrast scans were subtracted from post-contrast scans after which the percentage increase following gadolinium injection was calculated for the contralateral hemisphere (negative control set to 100 %), tumor tissue and extracranial muscle tissue (positive control) for each animal. Significant differences were determined by ANOVA testing (GraphPad PRISM, GraphPad Software, La Jolla, CA, USA) with $p < 0.05$.

Evans blue

A phototrombotic stroke was induced as described previously [16] as a positive control for Evans blue uptake and the disruption of the BBB. In short, the animal was sedated with isoflurane. After exposing the skull, the photosensitizer rose bengal (20 mg/kg, Sigma-Aldrich, St. Louis, MO, USA) was injected intravenously followed by photo-illumination of the right motor cortex with green light (wave length, 540 nm; bandwidth 80 nm) from a xenon light (model L-4887; Hamamatsu Photonics, Hamamatsu City, Japan) for 20 min with an irradiation intensity of 0.68 W/cm^2. Focal activation of the photosensitive dye results in local endothelial cell injury leading to microvascular thrombosis and circumscribed cortical infarctions. Afterwards, the mouse was allowed to recover. Within 24 h, Evans blue (4 µl/g of body weight of a 2 % Evans blue solution [3]) was administered i.v. and the mouse was perfused approximately 25 min post injection. At several time points, one animal from the GL261 tumor bearing group (week 2 and 4) and one animal from the Hs683 tumor bearing group (week 2, 4 and 5) was sacrificed similarly.

Endpoints

Animals were sacrificed when symptoms reached grade 3 out of 4 (grade 0 for healthy mice, grade 1 for slight unilateral paralysis, grade 2 for moderate unilateral paralysis and/or beginning hunchback, grade 3 for severe unilateral or bilateral paralysis and pronounced hunchback, and grade 4 for moribund mice) [17].

Histology

Animals were sacrificed by an overdose of Nembutal (250 µl, i.p., ceva, Libourne, France) and subsequently perfused with 4 % ice-cold paraformaldehyde (PFA) solution (Sigma-Aldrich). After overnight post-fixation in 4 % PFA, the brain tissue was kept in a 0.1 % sodium azide solution (Fluka, Sigma-Aldrich, Belgium) at 4 °C. Paraffin sections (5 µm thickness) were sliced and a Masson's trichrome staining and a GFAP staining were performed. In short, for the Masson's staining, sections were deparaffinized and rehydrated prior to hematoxylin, ponceau/fuchsine and aniline blue staining after which they were dehydrated and mounted with DPX (Sigma-Aldrich). For the GFAP staining, deparaffinization and rehydration were performed prior to staining. Subsequently, antigen retrieval was performed and sections were incubated overnight at 4 °C with the primary polyclonal rabbit anti-glial fibrillary acidic protein (GFAP) antibody (1/250, Dako-Z0334), followed by staining with the secondary Alexa Fluor®488 goat anti-rabbit IgG antibody (1/500, Invitrogen, A11034) for 30 min at room temperature and Hoechst (1/1000, Sigma-Aldrich, 33258) after which they were also dehydrated and mounted with Prolong® Gold antifade reagent(Invitrogen, P36930).

Results

GL261 glioblastoma mouse model

Injection of 2.5×10^5 GL261 cells in the striatum of C57BL6/J mice resulted in tumors with an average size of 76 ± 14 mm^3 at 5 weeks post injection (Fig. 1a). MR images of a representative GL261 tumor bearing animal are shown in Fig. 1b. Weekly MRI sessions showed an increased BBB disruption over time (Fig. 1c, d), starting already from week 2 post glioma induction. The relative signal intensity increased over time indicating progressing BBB disruption with tumor growth.

Furthermore, the characteristics of the developing tumor were evaluated more elaborately by histological analysis (Fig. 2). Masson's trichrome staining revealed tumor infiltration for small tumors into the normal brain parenchyma (a) whereas this was less apparent in larger tumors. Also nuclear atypia (Fig. 2 b1), mitosis (Fig. 2 b2) and extensive vascularization (Fig. 2 b3), all characteristics of glioblastoma were detected. Furthermore, histology showed both necrosis and apoptosis as tumors grew larger (Fig. 2c), which correlated with non-enhancing regions on MRI after gadolinium injection (Fig. 2d). Also a midline shift caused by the aggressive growth of the tumor was observed both on MRI and histology. Finally, GFAP staining proved negative (Fig. 2e).

Subsequently, one animal was sacrificed on week 2 and 4 post tumor injection after Evans blue injection to confirm loss of BBB integrity (Fig. 3) observed on MRI (Fig. 3a). Leakage of Evans blue (Fig. 3b) indeed confirmed BBB disruption as early as week 2 post glioma initiation.

Hs683 oligodendroglioma mouse model

Injection of 5×10^4 Hs683 cells in the striatum of Hsd:Athymic Nud-Foxn ^{1nu} mice resulted in tumor formation with an average tumor size of 244 ± 0.3 mm^3 at

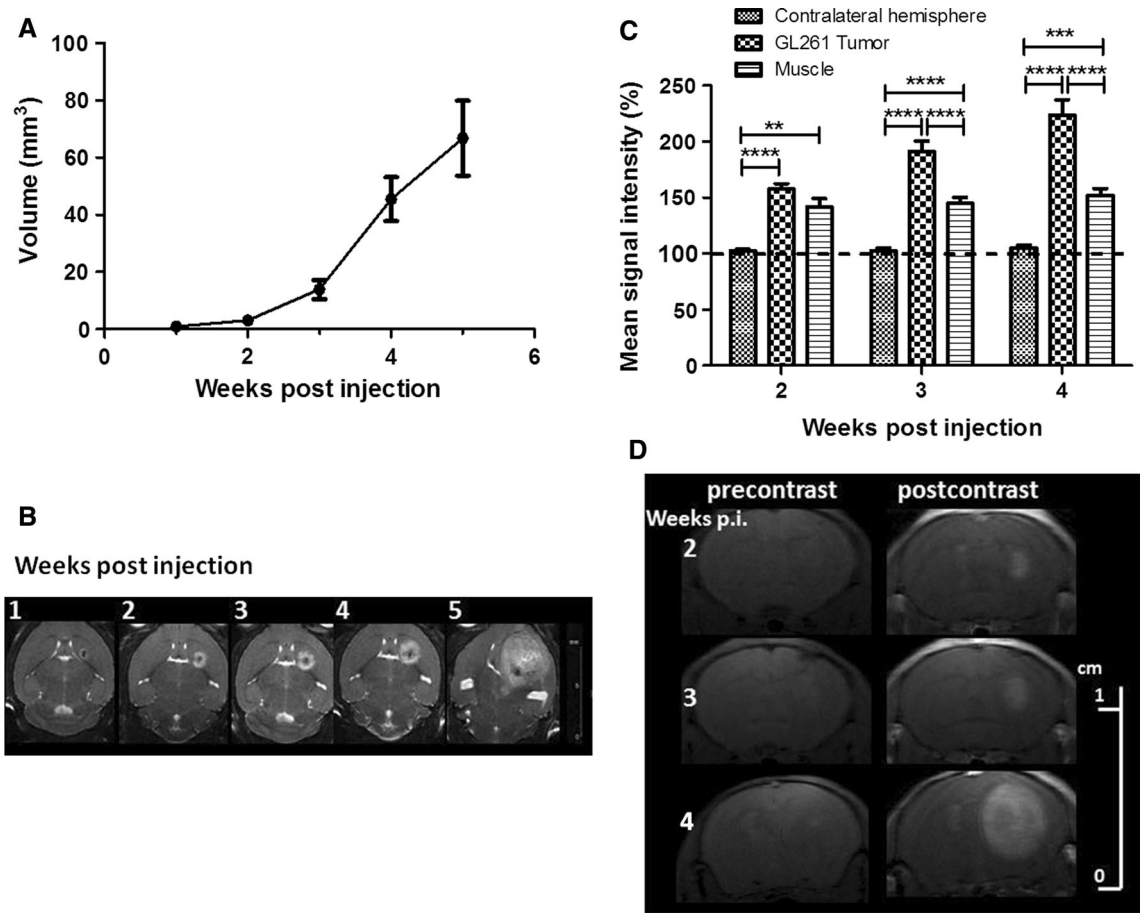

Fig. 1 BBB integrity assessment by contrast enhancement in T1 W MRI for GL261 tumors. **a** Tumors grow gradually over time until they reach an average size of 76 $mm^3 \pm 14$ at 5 weeks post injection (N = 12). **b** Example of tumor growth in a representative animal (T2 W MR image, coronal orientation). **c** Intravenous injections of gadolinium showed a loss of BBB integrity, which deteriorates over time (N = 11). **d** Example of contrast enhancement on T1 W MR images in the same animal mentioned in C over time. $*p < 0.05$, $**p < 0.01$, $***p < 0.001$, $****p < 0.0001$

8 weeks post injection (Fig. 4a). MR images of a representative Hs683 tumor bearing animal are shown in Fig. 4b. T1 W MR imaging following i.v. injection of gadolinium showed loss of the BBB integrity compared to the contralateral hemisphere (Fig. 4c). However, the relative changes in signal intensity compared to the contralateral hemisphere and the extracranial muscle tissue were much smaller than those observed for the GL261 tumors.

In contrast to the GL261 model, extensive heterogeneity was evident on T1 W post-contrast MR images in large Hs683 tumors (Fig. 4d), which was confirmed by T2 W MR images (Fig. 5a) and histological analysis (Fig. 5b, c). Masson's trichrome staining of paraffin embedded brains revealed large fluid filled cysts but no regions of pronounced necrosis or apoptosis. Many of the large fluid filled cysts also contained blood. Finally, GFAP staining was also negative for Hs683 tumors (Fig. 5d).

Subsequently, animals were sacrificed following Evans blue injections on weeks 2, 4 and 5 post tumor initiation to confirm the observations made by T1 W post-contrast MR images (Fig. 3c). Loss of BBB integrity in the Hs683 model could however not be shown at any of the mentioned time points by Evans blue (Fig. 3d), which is in line with the relatively small changes in the T1 W post-contrast MR images.

Discussion

In this study, the BBB integrity was assessed in two high grade glioma mouse models. One of the hallmarks of high grade gliomas is neovascularization [18], characterized by severe leakiness [19], which correlates with tumor grade and malignancy [4]. Furthermore, some experimental brain tumor treatments, using for instance systemically injected stem cells [11, 12] or administration of large or hydrophilic therapeutic molecules [13] could be hampered by incomplete BBB disruption, which might decrease treatment efficacy. It is therefore crucial to characterize tumor

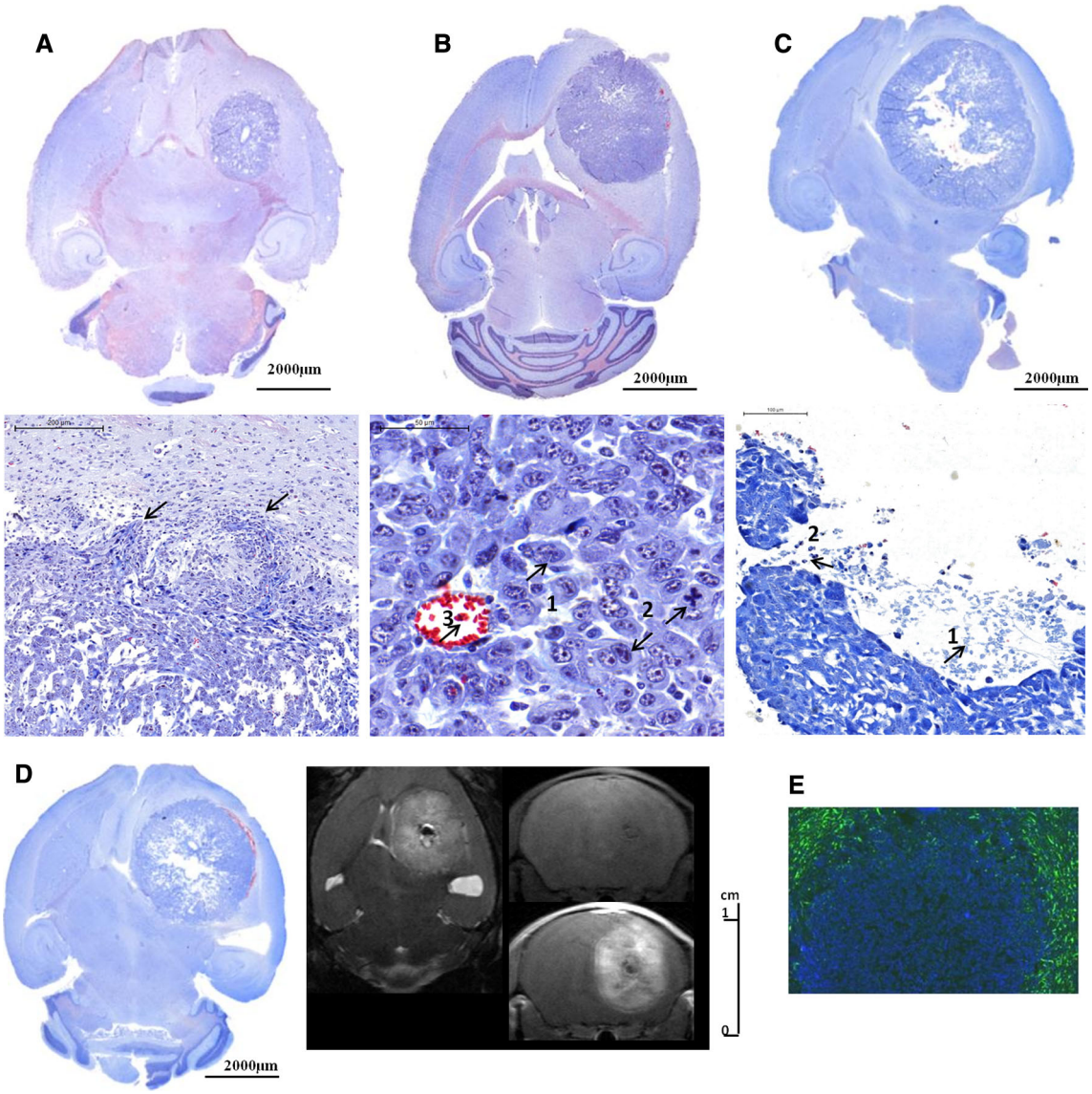

Fig. 2 Histological analysis of the GL261 tumors **a** Infiltration of the tumor cells into normal brain parenchyma was observed mainly for smaller tumors, whereas this was less apparent in larger tumors. **b** Several typical characteristics of glioblatoma were detected, such as nuclear atypia (1), mitosis (2) and the presence of extensive vascularization (3). **c** In very large tumors, necrosis (1) and apoptosis (2) became apparent in the centre of the tumors. **d** Central necrosis correlated with non-enhancing regions on MRI after gadolinium injections. Both on MRI and histology, a midline shift became apparent as tumors grew larger. **e** GFAP staining showed that the tumor is negative for the glial fibrillary acidic protein as no GFAP staining (*green*) could be detected in the tumor whereas it was stained with Hoechst (*blue*)

models very carefully before considering the assessment of possible treatment regimes. Here, we compared the assessment of BBB disruption by using CE-T1 W MRI and the high molecular weight marker Evans blue. While CE-T1 W MRI is common practice in the clinic, we have used MRI and Evans blue staining for the comparison of a frequently used experimental model (GL261) with a less frequently used, humanized model (Hs683).

One of the most used glioblastoma models in preclinical research is the GL261 model as it is a syngeneic and well characterized model with a very reproducible growth. In this model, BBB disruption was shown as soon as 2 weeks post tumor cell injection (2.5×10^5). Hereby, we confirmed the results obtained previously by Cha et al. [10] and proved that the applied methodology can be used to assess BBB disruption. Furthermore, we showed infiltration, mitosis, nuclear atypia and the presence of blood vessels in these tumors. Also a midline shift due to the aggressive growth of the tumor, causing elevated intracerebral pressure, was apparent both on MRI and histological analysis. GFAP staining was negative, which is consistent with previously published reports [14].

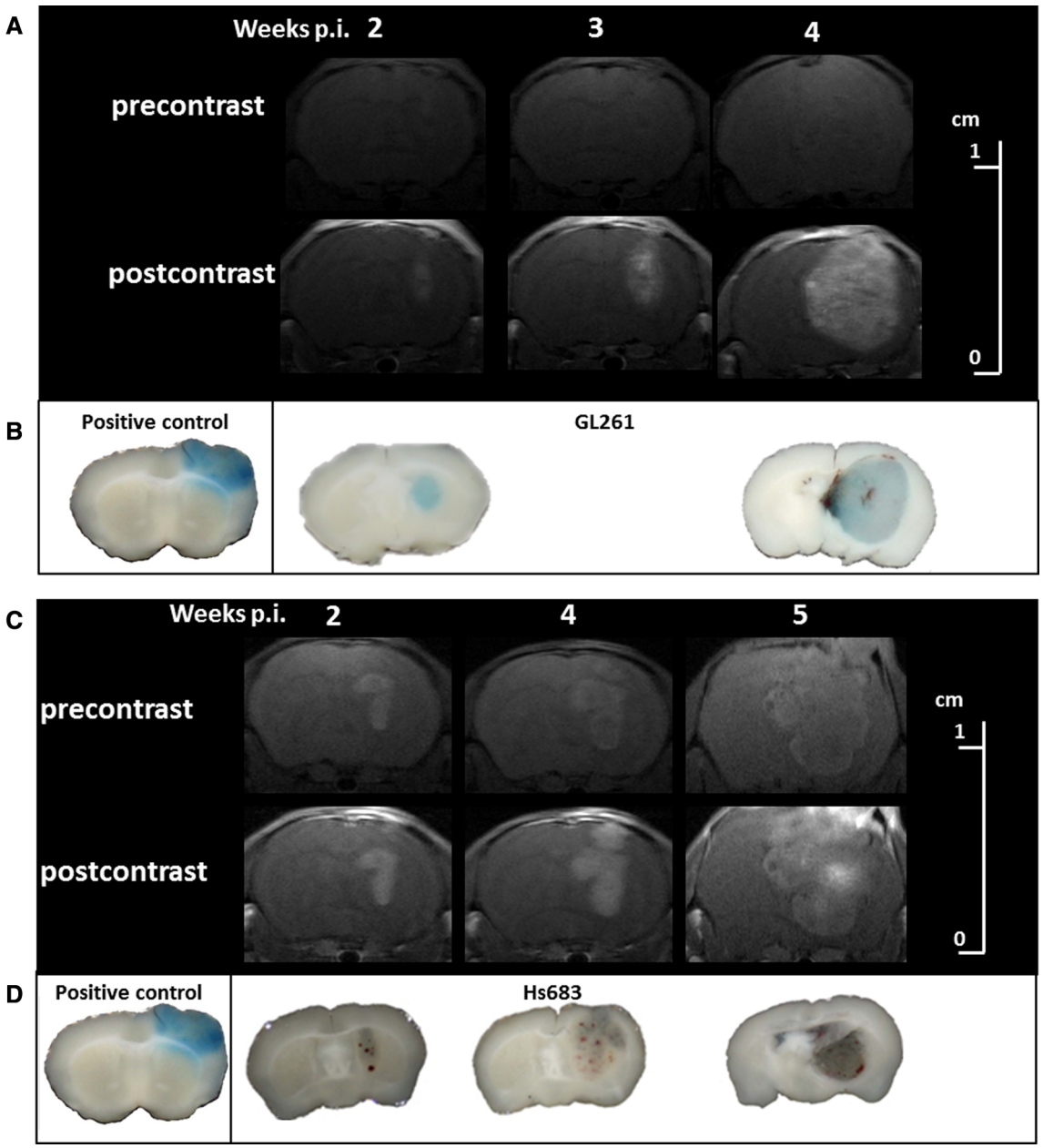

Fig. 3 BBB integrity assessment using Evans blue staining. **a** Contrast enhancement in T1 W MRI before and after gadolinium injection showed a loss of the BBB integrity in the GL261 model. **b** Sliced brains of Evans blue perfused animals confirmed BBB disruption in the GL261 model on both week 2 and week 4 post tumor injection. A phototrombotic stroked animal was used as a positive control for BBB disruption. **c** Contrast enhancement on T1 W MRI before and after gadolinium injection showed BBB disruption in the Hs683 model. **d** Sliced brains of animals receiving Evans blue prior to perfusion did not show BBB integrity lossfor any of the Hs683 tumor bearing animals on weeks 2, 3, 4 or 5 post tumor initiation. A phototrombotic stroked animal was used as a positive control to confirm BBB disruption

Translation of the results obtained in animal models is however not straight forward [20]. We have used a humanized animal model (transplantation of human tumor cells (Hs683) in an immune-suppressed animal), which is less extensively characterized.

The BBB integrity of the GL261 model was compared with the Hs683 model. These tumors grew very large before resulting in grade 3 symptoms. Furthermore, large fluid filled cysts appeared both on MRI and histology. These tumors were also GFAP negative, which is consistent with previous reports from Belot et al., who observed very low levels of GFAP mRNA [21]. Lamoral-Theys et al. proposed that this oligodendroglioma model could represent a glioblastoma with an oligodendroglial origin [22]. To our knowledge there are however no reports on the BBB status in this model. CE-T1 W MRI showed a

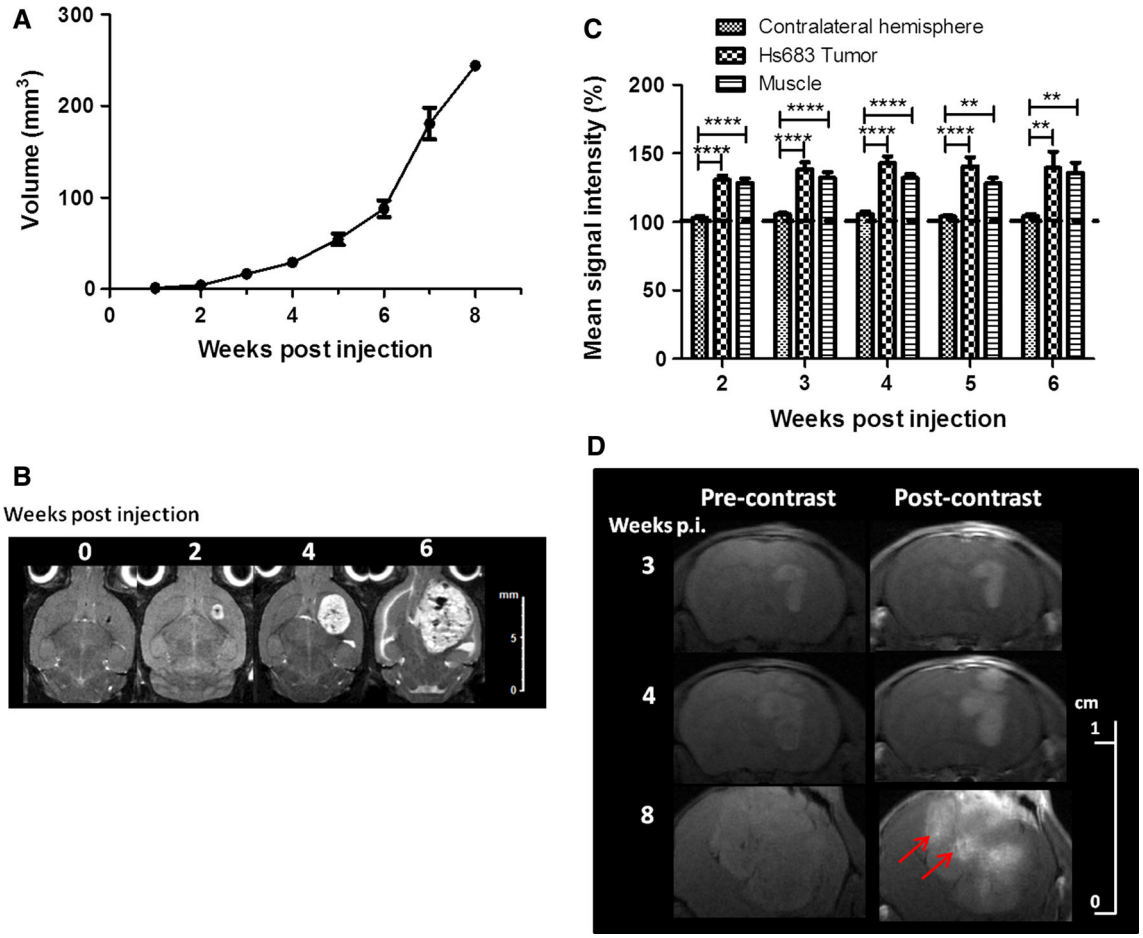

Fig. 4 BBB integrity assessment by MRI for the Hs683 tumor model. **a** Tumors grew gradually over time until they reached an average size of 244 ± 0.3 mm^3 at 8 weeks post injection (N = 22). **b** Example of Hs683 tumor growth in a representative animal (T2 W MR image, coronal orientation). **c** Intravenous injections of gadolinium showed a loss of BBB integrity starting from week 2 post tumor initiation (N = 22). **d** Intratumoral heterogeneity of the integrity of the BBB causes differences in maximal signal intensity on later time points. Areas with high (red arrows) and low signal intensities can be seen within a single tumor. $*p < 0.05$, $**p < 0.01$, $***p < 0.001$, $****p < 0.0001$

heterogeneous contrast enhancement of lower relative signal intensity changes in the tumor region when compared to the GL261 model. In contrast, Evans blue did not give evidence for BBB disruption at any time point. Although loss of BBB integrity is a general characteristic of glioblastoma, little is known about the actual mechanisms involved in the BBB disruption. One hypothesis is however that increased MMP3 activity, followed by agrin degradation results in loss of astrocyte polarity causing BBB integrity loss [23]. BBB disruption on MRI but not after Evans blue injection could be explained by an incomplete BBB disruption as gadolinium chelates (Dotarem®) and Evans blue bound to albumin have different molecular weights of 562 and 69,000 Da, respectively. If the BBB is not fully disrupted, larger molecules would have more difficulty passing the BBB, which would explain the negative Evans blue staining.

These results might aid researchers to assess mechanisms of novel therapeutic approaches where the breakdown of the BBB might be of importance. For example, Mathieu et al. studied the combination of chemotherapeutics (Temozolomide) and anti-angiogenic compounds (Bevacizumab) where Temozolomide is able to cross the BBB (MW Temozolomide: 194 Da, MW Dotarem: 562 Da) but Bevacizumab would not be able to cross the BBB (MW Bevacizumab = 149 kDa, MW albumin-bound Evans blue = 69 kDa) but may still exert its anti-angiogenic effect from within tumor vessels [24].

In conclusion, the Hs683 model should be used with caution when using therapeutic products that normally do not pass the BBB easily.

Finally, a difference in heterogeneity of the BBB disruption was observed by CE-T1 W MR imaging of the two glioblastoma models. Glioblastomas are known for their

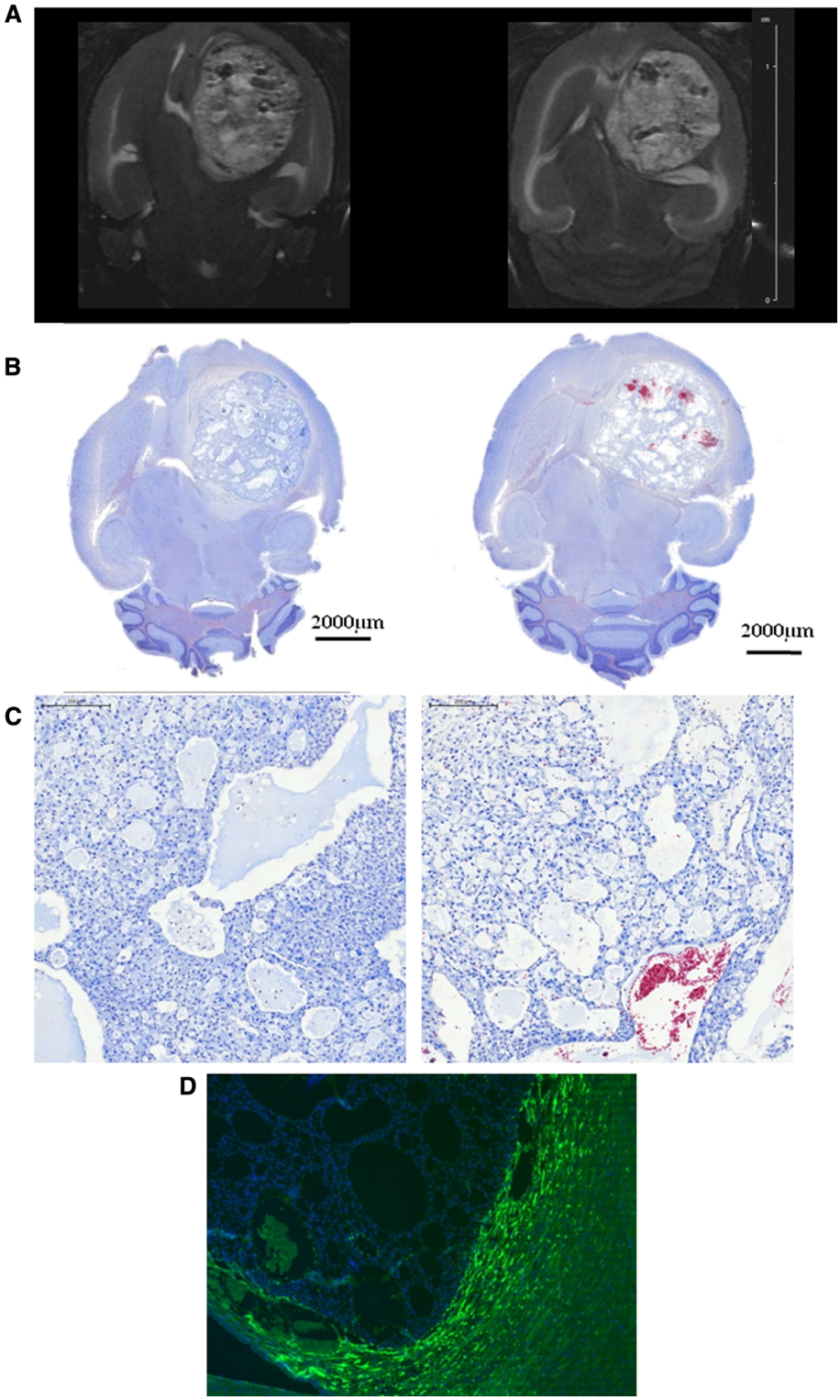

Fig. 5 Histological analysis of Hs683 tumors. **a** T2 W MR images (coronal orientation) of Hs683 tumor bearing animals at week 6 post tumor initiation. **b** Corresponding 5 µm thick paraffin embedded brain sections stained with a Masson's trichrome staining showed large fluid filled cyst formation and blood vessels which corresponded to respectively hyper- and hypointens areas on T2 W MR images shown in **a**. **c** Examination of the tumors did not show pronounced necrosis/apoptosis (× 10). **d** GFAP staining was negative for Hs683 tumors (× 5). (Hoechst = *blue*)

inter- and intratumoral heterogeneity [25, 26], which logically results in regional differences of contrast enhancement. Therefore, we have analyzed only enhancing regions for our semi-quantitative assessment of the BBB disruption, which are also the regions selected in the clinic for histopathological evaluation [27]. The GL261 tumors appeared relatively homogenous on CE-T1 W MR imaging, even as tumors grew very large. Only very few regions

did not enhance on T1 W MRI, representing necrotic regions, which was also confirmed on histological sections. The Hs683 tumors became however increasingly heterogeneous over time, with the presence of very large fluid filled cysts and microbleedings shown both on T2 W MR images and histological sections, which also explains their heterogeneous contrast enhancement on CE-T1 W MR images.

Recently, macromolecular Gadolinium-chelates, such as albumin bound chelates, have been investigated as contrast agents for BBB disruption [28]. Although promising results have been reported, further feasibility studies are required as preliminary results show that longer delay times of up to 4 h are required prior to imaging for obtaining reliable results [28].

In conclusion, in this study the BBB integrity of two high-grade glioma mouse models was assessed by means of CE-T1 W MR imaging and Evans blue staining. The BBB integrity data from both methods was concurrent for the GL261 glioblastoma model, clearly indicating BBB integrity loss as soon as 2 weeks post tumor cell injection. In contrast, the data obtained for the Hs683 oligodendroglioma model showed a limited BBB disruption based on the high molecular weight Evans blue staining and a reduced uptake of low molecular weight gadolinium chelates as indicated by the CE-T1 W MRI. These results clearly indicate the importance of checking the BBB integrity status using different methods. This is in particular of importance for the assessment of therapeutic molecules and the selection of appropriate animal models. Care should be taken with the appropriate assessment of the BBB disruption prior to commencing therapeutic investigations.

Acknowledgements We would like to thank Prof. Van Gool and Prof. Kiss for supplying us with GL261 and Hs683 tumor cell lines. Furthermore, we would like to thank Prof. Lambrichts and Ms. Santermans for the use of the equipment of the lab of Histology at Hasselt University. Finally, we would also like to thank Prof Verfaillie for logistic support. We are grateful for the financial support from the European commission for EC-FP7 HEALTH.2011.2.2.1–2 (INMiND), from the Flemish government for FWO G0A7514 N, IWT-SBO MIRIAD (130065) and IWT-BRAINSTIM (060838) and from the University of Leuven for the program financing IMIR (PF 10/017).

Conflict of interest The authors declare that there are no conflicts of interest.

References

1. Zagzag D et al (2000) Vascular apoptosis and involution in gliomas precede neovascularization: a novel concept for glioma growth and angiogenesis. Lab Invest 80(6):837–849
2. Wesseling P, Ruiter DJ, Burger PC (1997) Angiogenesis in brain tumors; pathobiological and clinical aspects. J Neurooncol 32(3):253–265
3. Kaya M, Ahishali B (2011) Assessment of permeability in barrier type of endothelium in brain using tracers: evans blue, sodium fluorescein, and horseradish peroxidase. Methods Mol Biol 763:369–382
4. Roberts HC et al (2002) Quantitative estimation of microvascular permeability in human brain tumors: correlation of dynamic Gd-DTPA-enhanced MR imaging with histopathologic grading. Acad Radiol 9(Suppl 1):S151–S155
5. Just M et al (1991) MRI-assisted radiation therapy planning of brain tumors–clinical experiences in 17 patients. Magn Reson Imaging 9(2):173–177
6. Roberts HC et al (2002) Dynamic, contrast-enhanced CT of human brain tumors: quantitative assessment of blood volume, blood flow, and microvascular permeability: report of two cases. AJNR Am J Neuroradiol 23(5):828–832
7. Nomura T, Inamura T, Black KL (1994) Intracarotid infusion of bradykinin selectively increases blood-tumor permeability in 9L and C6 brain tumors. Brain Res 659(1–2):62–66
8. Preston E, Webster J (2002) Differential passage of [14C]sucrose and [3H]inulin across rat blood-brain barrier after cerebral ischemia. Acta Neuropathol 103(3):237–242
9. Loveless ME et al (2011) A quantitative comparison of the influence of individual versus population-derived vascular input functions on dynamic contrast enhanced-MRI in small animals. Magn Reson Med 67(1):226–236
10. Cha S et al (2003) Dynamic, contrast-enhanced perfusion MRI in mouse gliomas: correlation with histopathology. Magn Reson Med 49(5):848–855
11. Matuskova M et al (2009) HSV-tk expressing mesenchymal stem cells exert bystander effect on human glioblastoma cells. Cancer Lett 290(1):58–67
12. Hata, N., et al., 2010, Platelet-derived growth factor BB mediates the tropism of human mesenchymal stem cells for malignant gliomas. Neurosurgery. **66**(1): p. 144–156; discussion 156–157
13. Pardridge WM (2007) Drug targeting to the brain. Pharm Res 24(9):1733–1744
14. Szatmari T et al (2006) Detailed characterization of the mouse glioma 261 tumor model for experimental glioblastoma therapy. Cancer Sci 97(6):546–553
15. Branle F et al (2002) Evaluation of the efficiency of chemotherapy in in vivo orthotopic models of human glioma cells with and without 1p19q deletions and in C6 rat orthotopic allografts serving for the evaluation of surgery combined with chemotherapy. Cancer 95(3):641–655
16. Vandeputte C et al (2011) Characterization of the inflammatory response in a photothrombotic stroke model by MRI: implications for stem cell transplantation. Mol Imaging Biol 13(4):663–671
17. Maes W et al (2009) DC vaccination with anti-CD25 treatment leads to long-term immunity against experimental glioma. Neuro Oncol 11(5):529–542
18. Jain RK et al (2007) Angiogenesis in brain tumours. Nat Rev Neurosci 8(8):610–622
19. Lee SW et al (2006) Blood-brain barrier interfaces and brain tumors. Arch Pharm Res 29(4):265–275
20. Juratli TA, Schackert G, Krex D (2013) Current status of local therapy in malignant gliomas—a clinical review of three selected approaches. Pharmacol Ther 139(3):341–358
21. Belot N et al (2001) Molecular characterization of cell substratum attachments in human glial tumors relates to prognostic features. Glia 36(3):375–390
22. Lamoral-Theys D et al (2010) Long-term temozolomide treatment induces marked amino metabolism modifications and an increase in TMZ sensitivity in Hs683 oligodendroglioma cells. Neoplasia 12(1):69–79
23. Wolburg H et al (2012) The disturbed blood-brain barrier in human glioblastoma. Mol Aspects Med 33(5–6):579–589

24. Mathieu V et al (2008) Combining bevacizumab with temozolomide increases the antitumor efficacy of temozolomide in a human glioblastoma orthotopic xenograft model. Neoplasia 10(12):1383–1392
25. Sturm D et al (2012) Hotspot mutations in H3F3A and IDH1 define distinct epigenetic and biological subgroups of glioblastoma. Cancer Cell 22(4):425–437
26. Szerlip NJ et al (2011) Intratumoral heterogeneity of receptor tyrosine kinases EGFR and PDGFRA amplification in glioblastoma defines subpopulations with distinct growth factor response. Proc Natl Acad Sci USA 109(8):3041–3046
27. Barajas RF Jr et al (2012) Regional variation in histopathologic features of tumor specimens from treatment-naive glioblastoma correlates with anatomic and physiologic MR Imaging. Neuro Oncol 14(7):942–954
28. Kremer S et al (2013) Evaluation of an albumin-binding gadolinium contrast agent in multiple sclerosis. Neurology 81(3): 206–210